

---

# Simple and Effective VAE Training with Calibrated Decoders

---

Oleh Rybkin<sup>1</sup> Kostas Daniilidis<sup>1</sup> Sergey Levine<sup>2</sup>

<sup>1</sup> University of Pennsylvania <sup>2</sup> UC Berkeley

## Abstract

Variational autoencoders (VAEs) provide an effective and simple method for modeling complex distributions. However, training VAEs often requires considerable hyperparameter tuning, and often utilizes a heuristic weight on the prior KL-divergence term. In this work, we study how the performance of VAEs can be improved while not requiring the use of this heuristic hyperparameter, by learning calibrated decoders that accurately model the decoding distribution. While in some sense it may seem obvious that calibrated decoders should perform better than uncalibrated decoders, much of the recent literature that employs VAEs uses uncalibrated Gaussian decoders with constant variance. We observe empirically that the naïve way of learning variance in Gaussian decoders does not lead to good results. However, other calibrated decoders, such as discrete decoders or learning shared variance can substantially improve performance. To further improve results, we propose a simple but novel modification to the commonly used Gaussian decoder, which represents the prediction variance non-parametrically. We observe empirically that using the heuristic weight hyperparameter is not necessary with our method. We analyze the performance of various discrete and continuous decoders on a range of datasets and several single-image and sequential VAE models.<sup>1</sup>

## 1 Introduction

Deep density models based on the variational autoencoder (VAE) [29, 47] have found ubiquitous use in probabilistic modeling and representation learning as they are both conceptually simple and are able to scale to very complex distributions and large datasets. These VAE techniques are used for tasks such as future frame prediction [8], image segmentation [31], generating sentences [7], speech [11], sketches [21], and music [14], as well as model-based reinforcement learning [22], and representation learning [34, 19, 52]. However, in practice, many of these approaches require careful manual tuning of the balance between two terms that correspond to distortion and rate from information theory [3]. This balance trades off fidelity of reconstruction and quality of samples from the model: a model with low rate would not contain enough information to reconstruct the data, while allowing the model to have high rate might lead to unrealistic samples from the prior as the KL-divergence constraint becomes weaker [2, 3, 26]. While a proper variational lower bound does not expose any free parameters to control this tradeoff, many prior works heuristically introduce a weight on the prior KL-divergence term, often denoted  $\beta$ . Usually,  $\beta$  needs to be tuned for every dataset and model variant as a hyperparameter, which slows down development and can lead to poor performance as finding the optimal value is often prohibitively computationally expensive. Moreover, using  $\beta \neq 1$  precludes the appealing interpretation of the VAE objective as a bound on the data likelihood, and is undesirable for applications like density modeling.

Much of the recent literature that employs VAEs uses uncalibrated decoding distributions, such as Gaussian without learned variance, where the decoder only outputs the mean parameter [8, 13, 34, 6,

---

<sup>1</sup>Project website: <https://orybkin.github.io/sigma-vae/>

33, 23, 45, 54, 42, 24]. The mean squared error loss on this mean corresponds to a log-likelihood with an implicit, constant variance. We observe empirically that the performance of these VAE methods can be improved substantially by using a decoding distribution that can produce calibrated probabilities for the decoding distribution. In our experiments, this removes the need to tune the additional parameter  $\beta$ . Indeed, we note that the entropy of the decoding distribution controls the mutual information  $I(x; z)$ . Calibrated decoders allow the model to control this mutual information automatically, instead of relying on manual tuning. While in some sense it may seem obvious that a calibrated decoder should be more effective than an uncalibrated one, we observe empirically that simply learning the variance of a Gaussian distribution as another output from the decoder generally performs poorly in practice, perhaps explaining in part the popularity of heuristically weighting the KL-divergence term and not utilizing a learned variance.

However, we observe that simple modifications can be used to produce calibrated decoder probabilities and substantially improve the quality of VAE samples and reconstructions. First, we observe that discrete decoders, formulated as  $n$ -way classifiers on pixel intensities, substantially outperform naïve unit variance Gaussian decoders, but at a considerable cost in memory and computation, making it difficult to train models on videos or high-resolution images. We then describe a modification to the commonly used Gaussian decoder, where a scalar variance shared across images is learned. This results in stable training and performance comparable or higher than that of the discrete decoder. Finally, we propose a simple but novel technique for optimizing this variance in which it is represented non-parametrically. We call the resulting approach to learning the Gaussian variance the  $\sigma$ -VAE. In our experiments, the  $\sigma$ -VAE outperforms the alternative of learning the variance through gradient descent, while being simpler to implement and extend.

Our contributions are as follows. First, we provide an analysis of calibrated decoders for improved VAE training. Specifically, we examine a range of decoders and show that learning calibrated decoding distributions such as discrete distributions or Gaussian distributions with learned variance balances the VAE objective automatically, allowing to not use the additional hyperparameter  $\beta$ . We analyze the impact of learning a calibrated decoder on the information-theoretic properties of the representation, and further address the common challenges in learning calibrated decoders that prevent practitioners from using it and show that simple modifications can rectify them. Second, we propose a novel method for learning calibrated Gaussian decoders that leverages an analytic solution for the variance and further improves learning. We validate our results on several VAE and sequence VAE models and a range of image and video datasets.

## 2 Related Work

Prior work on variational autoencoders has studied a number of different decoder parameterizations. Kingma and Welling [29], Rezende et al. [47] use the Bernoulli distribution for the binary MNIST data and Kingma and Welling [29] use Gaussian distributions with learned variance parameter for grayscale images. However, modelling images with continuous distributions is prone to instability as the variance can converge to zero [46, 38, 12]. Some work has attempted to rectify this problem by adding uniform noise to ground truth data [18], or optimizing the variance in a two-stage procedure [5]. Additionally, different choices for representing such variance exist, including diagonal covariance [29, 51, 48], or a single shared parameter [30, 12, 15, 46]. We analyze these and notice that learning a single variance parameter shared across images leads to numerically stable training and good performance, without resorting to adding noise or even clipping the variance; and further improve the estimation of this variance with a non-parametric solution.

Early work on discrete VAE decoders for color images attempted to model them with the Bernoulli distribution, treating the color intensities as probabilities [17]. Further work has explored various parameterizations based on discretized continuous distributions, such as discretized logistic [30]. More recent work has improved expressivity of the decoding distributions with a mixture of discretized logistics [9, 37]. However, these models also employ powerful autoregressive decoders [9, 20, 37], and the latent variables in these models may not represent all of the significant factors of variation in the data, as some factors can instead be modeled internally by the autoregressive decoder [3].<sup>2</sup>

---

<sup>2</sup>BIVA [37] uses the Mixture of Logistics decoder proposed in [50] that produces the channels for each pixel autoregressively, see also App C.

While a range of calibrated decoding techniques exist, we observe that, outside the core generative modeling community, uncalibrated decoders are ubiquitous. They are used in work on future frame prediction [13, 8, 33, 6], image segmentation [31], image-to-image translation [54], generating 3D human pose [42], as well as model-based reinforcement learning [24, 23, 22], and representation learning [34, 52, 45]. The majority of these works utilize the heuristic hyperparameter  $\beta$  instead, which is undesirable both as the resulting objective is no longer a bound on the log-likelihood, and as the hyperparameter  $\beta$  usually requires extensive tuning. In this work, we analyze the common pitfalls of using calibrated decoders that may have prevented the practitioners from using them, propose a simple and effective non-parametric way of learning such calibrated distribution, and provide a comprehensive experimental evaluation of different decoding distributions.

Alternative discussions of the hyperparameter  $\beta$  are presented by Zhao et al. [53], Higgins et al. [26], Alemi et al. [3], Achille and Soatto [2], who show that it controls the amount of information in the latent variable,  $I(x; z)$ . Peng et al. [43], Rezende and Viola [46] further discuss constrained optimization objectives for VAEs, which also yield a similar hyperparameter. Here, we focus on  $\beta$ -VAEs with Gaussian decoders with constant variance, as commonly used in recent work, and show that the hyperparameter  $\beta$  can be incorporated in the decoding likelihood for these models.

### 3 Calibrated Decoding Distributions

The generative model of a VAE [29, 47] with parameters  $\theta$  is specified with a prior distribution over the latent variable  $p_\theta(z)$ , commonly unit Gaussian, and a decoding distribution  $p_\theta(x|z)$ , which for color images is commonly a conditional Gaussian parameterized with a neural network. We would like to fit this generative model to a given dataset by maximizing the evidence lower bound (ELBO [39, 27, 29, 47]), which uses an approximate posterior distribution  $q_\phi(z|x)$ , also commonly a conditional Gaussian specified with a neural network. In this work, we focus on the form of the decoding distribution  $p_\theta(x|z)$ . To achieve the best results, we want a decoding distribution that represents the required probability  $p(x|z)$  accurately, that is, we want the decoding distribution to be *calibrated* in the statistical sense. In this section, we will review and analyze various choices of decoding distributions that enable better decoder calibration, including expressive decoding distributions that can represent both the prediction of the image and the uncertainty about such prediction, or even multimodal predictions.

#### 3.1 Gaussian Decoders

We first analyse the commonly used Gaussian decoders. We note that the commonly used MSE reconstruction loss between the reconstruction  $\hat{x}$  and ground truth data  $x$  is equivalent to the negative log-likelihood objective with a Gaussian decoding distribution with constant variance:

$$-\ln p(x|z) = \frac{1}{2} \|\hat{x} - x\|^2 + D \ln \sqrt{2\pi} = \frac{1}{2} \|\hat{x} - x\|^2 + c = \frac{D}{2} \text{MSE}(\hat{x}, x) + c,$$

where  $p(x|z) \sim \mathcal{N}(\hat{x}, I)$ , the prediction  $\hat{x}$  is produced with a neural network  $\hat{x} = \mu_\theta(z)$ , and  $D$  is the dimensionality of  $x$ .

This demonstrates a drawback of methods that rely simply on the MSE loss [8, 13, 34, 23, 45, 54, 24], as it is equivalent to assuming a particular, constant variance of the Gaussian decoding distribution. By learning this variance, we can achieve much better performance due to better calibration of the decoder. There are several ways in which we can specify this variance. An expressive way to specify the variance is to specify a diagonal covariance matrix for the image, with one value per pixel [29, 51, 48]. This can be done, for example, by letting a neural network  $\sigma_\theta$  output the diagonal entries of the covariance matrix given a latent sample  $z$ :

$$p_\theta(x|z) \sim \mathcal{N}(\mu_\theta(z), \sigma_\theta(z)^2). \quad (1)$$

This parameterization of the decoding distribution outputs one variance value per each pixel and channel. While powerful, we observe in Section 5.3 that this approach attains suboptimal performance, and is moreover prone to numerical instability. Instead, we will find experimentally that a simpler parameterization, in which the covariance matrix is specified with a single shared [30, 12, 15, 46] parameter  $\sigma$  as  $\Sigma = \sigma I$  often works better in practice:

$$p_{\theta, \sigma}(x|z) \sim \mathcal{N}(\mu_\theta(z), \sigma^2 I). \quad (2)$$

The parameter  $\sigma$  can be optimized together with parameters of the neural network  $\theta$  with gradient descent. Of particular interest is the interpretation of this parameter. Writing out the expression for the decoding likelihood, we obtain

$$-\ln p(x|z) = \frac{1}{2\sigma^2} \|\hat{x} - x\|^2 + D \ln \sigma \sqrt{2\pi} = \frac{1}{2\sigma^2} \|\hat{x} - x\|^2 + D \ln \sigma + c = D \ln \sigma + \frac{D}{2\sigma^2} \text{MSE}(\hat{x}, x) + c.$$

The full objective of the resulting Gaussian  $\sigma$ -VAE is:

$$\mathcal{L}_{\theta, \phi, \sigma} = D \ln \sigma + \frac{D}{2\sigma^2} \text{MSE}(\hat{x}, x) + D_{KL}(q(z|x) || p(z)). \quad (3)$$

Note that  $\sigma$  may be viewed as a weighting parameter between the MSE reconstruction term and the KL-divergence term in the objective. Moreover, this objective explicitly specifies how to select the optimal variance: the variance should be selected to minimize the (weighted) MSE loss while also minimizing the logarithm of the variance.

**Connection to  $\beta$ -VAE.** The  $\beta$ -VAE objective [26] for a Gaussian decoder with unit variance is:

$$\mathcal{L}^\beta = \frac{D}{2} \text{MSE}(\hat{x}, x) + \beta D_{KL}(q(z|x) || p(z)). \quad (4)$$

We see that it can be interpreted as a particular case of the objective (3), where the variance is constant and the term  $D \ln \sigma$  can be ignored during optimization. The  $\beta$ -VAE objective is then equivalent to a  $\sigma$ -VAE with a constant variance  $\sigma = \sqrt{\beta/2}$  (for a particular learning rate setting). In recent work [54, 13, 34],  $\beta$ -VAE models are often used in this exact regime. By tuning the  $\beta$  term, practitioners are able to tune the variance of the decoder, manually producing a more calibrated decoder. As we will show in our experiments, the variance  $\sigma$  can instead simply be learned end-to-end, removing the need to manually select  $\beta$ .

An alternative discussion of this connection in the context of linear VAEs is also presented by Lucas et al. [36]. While the  $\beta$  term is not necessary for good performance if the decoder is calibrated, it can still be employed if desired, such as when the aim is to attain better disentanglement [26] or a particular rate-distortion tradeoff [3]. However, we found that with calibrated decoders, the best sample quality is obtained when  $\beta = 1$ .

**Loss implementation details.** For the correct evidence lower bound computation, it is necessary to add the values of the MSE loss and the KL divergence across the dimensions. We observe that common implementations of these losses [13, 1, 41] use averaging instead, which will lead to poor results if the number of image dimensions is significantly different from the number of the latent dimensions. While this can be conveniently ignored in the  $\beta$ -VAE regime, where the balance term is tuned manually anyway, for the  $\sigma$ -VAE it is essential to compute the objective value correctly.

**Variance implementation details.** Since the variance is non-negative, we parameterize it logarithmically as  $\sigma^2 = e^{2\lambda}$ , where  $\lambda$  is the logarithm of the standard deviation. For some models, such as per-pixel variance decoders, we observed that it is necessary to restrict the variance range for numerical stability. We do so by using the soft clipping operations proposed by Chua et al. [10]:

$$\lambda := \lambda_{\max} - \text{softplus}(\lambda_{\max} - \lambda); \quad \lambda := \lambda_{\min} + \text{softplus}(\lambda - \lambda_{\min}).$$

We observe that setting  $\lambda_{\min} = -6$  to lower bound the standard deviation to be at least half of the distance between allowed color values works well in practice. We also observe that this clipping is unnecessary when learning a shared  $\sigma$  value.

### 3.2 Discrete Decoders

It is possible to use discrete decoding distributions to generate images, as color values are commonly restricted to a fixed set of integer pixel intensities (e.g. 0..255). In the most general case, a discrete decoding distribution factorized per each pixel and channel would be specified by a probability mass vector  $\hat{x}$  with 256 entries, one per each possible intensity value, similarly to a per-pixel classifier of the intensity value. We can implement it with a soft-max layer, yielding the following log-likelihood loss (sometimes called the cross-entropy loss) for a true pixel with intensity  $i$ :

$$-\ln p(x|z) = -\ln \frac{\exp(\hat{x}_i)}{\sum_j \exp(\hat{x}_j)},$$

We will evaluate these and further choices of discrete decoders, described in Appendix C.

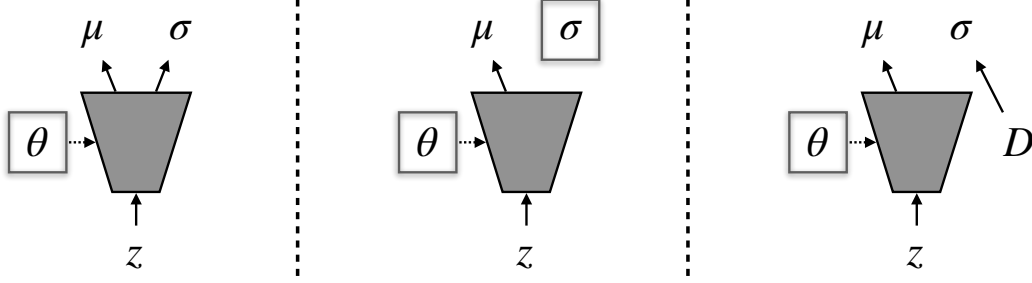


Figure 1: Different types of calibrated decoders for Gaussian VAE, model parameters are denoted with enclosing squares. Left: both the mean  $\mu$  and the variance  $\sigma$  are output by a neural network with parameters  $\theta$ . Center:  $\sigma$ -VAE with shared variance, the mean is output by a neural network with parameters  $\theta$ , but the variance is itself a global parameter. Right: the proposed optimal  $\sigma$ -VAE, the mean is output by a neural network with parameters  $\theta$ , and the variance is represented non-parametrically and computed from the training data  $D$ .

#### 4 Optimal Variance Estimation for Calibrated Gaussian Decoders

In this section, we propose a simple but novel non-parametric way of obtaining a calibrated decoder for continuous distributions that further improves performance. The Gaussian decoders with learned variance described in Section 3.1 are calibrated and work better than naïve unit variance decoders. However, for  $\sigma$ -VAE optimized with gradient descent or Adam [28], we observe that careful learning rate tuning can yield significantly better performance, which is in line with prior work that reported poor performance of gradient descent for optimizing Gaussian distributions [4, 44]. A smaller learning rate often produces better performance, but slows down the training, as the likelihood values  $p(x|z)$  will be very suboptimal in the beginning. Instead, here we propose an analytic solution for the value of  $\sigma$ , which represents it non-parametrically and does not require gradient descent.

The maximum likelihood estimate of the variance given a known mean is the average squared distance from the mean:

$$\sigma^* = \arg \max_{\sigma} \mathcal{N}(x|\mu, \sigma^2 I) = \text{MSE}(x, \mu), \quad (5)$$

where  $\text{MSE}(x, \mu) = \frac{1}{D} \sum_i (x_i - \mu_i)^2$ , and  $D$  is the dimensionality of  $x$ . Eq. 5 can be easily shown using manual differentiation, and is a generalization of the fact that the MLE estimate of the variance is the sample variance.

The optimal variance for the decoder distribution under the maximum likelihood criterion is then simply the average MSE loss. We leverage this to create an optimal analytic solution for the variance. In the batch setting, the optimal variance would be simply the MSE loss, and can be updated after every gradient update for the other parameters of the decoder. In the mini-batch setting, we use a batchwise estimate of the variance computed for the current minibatch. At test time, a running average of the variance over the training data is used. This method, which we call *optimal  $\sigma$ -VAE*, allows us to learn very efficiently as we use the optimal variance estimate at every training step. It is also non-parametric, as the variance is simply computed from training data whenever needed. This often makes it easier to implement, as no separate optimizer for the variance parameter is needed. If the variance is not needed at test time, it can also be simply discarded after training.

**Per-image optimal  $\sigma$ -VAE.** The method which we just described uses a single variance value shared across all data points. However, the optimal  $\sigma$ -VAE also allows more powerful variance estimates, such as learning a variance value per each pixel, or even a variance value per each image, the difference in implementation simply being the dimensions across which the averaging in Equation 5 operates. We observe that these versions can be more powerful, however, for the case of the per-image  $\sigma$ -VAE, the estimate of the variance is unavailable at test time since computing it requires optimizing the variance on that particular test image.

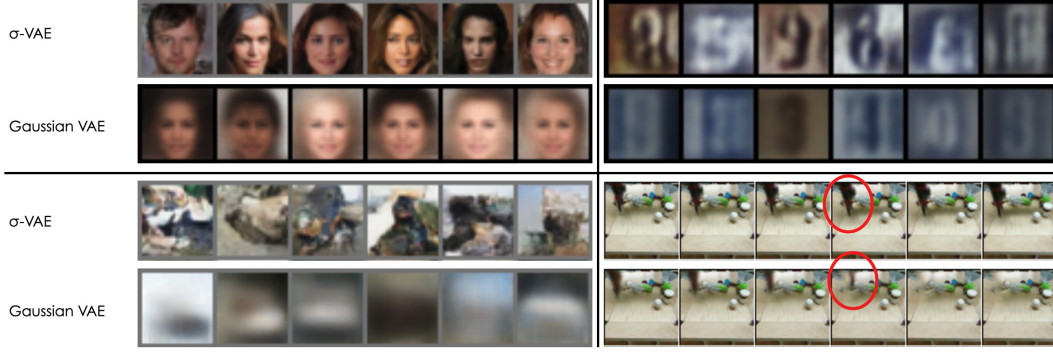


Figure 2: Images or videos (bottom right) sampled from the proposed optimal  $\sigma$ -VAE and a unit variance Gaussian VAE models. The Gaussian VAE does not have a means to control the expressivity of the latent variable and produces suboptimal, blurry samples. The  $\sigma$ -VAE controls the expressivity by learning a calibrated decoder, and produces higher quality sequences on all datasets.

## 5 Experimental Results

We now provide an empirical analysis of different decoding distributions, and validate the benefits of our  $\sigma$ -VAE approach. We use a small convolutional VAE model on SVHN [40], a larger hierarchical HVAE model [37] on the CelebA [35] and CIFAR [32] datasets, and a sequence VAE model called SVG [13] on the BAIR Pushing dataset [16]. We evaluate the ELBO values as well as visual quality measured by the Fréchet Inception Distance (FID [25]). Images are  $28 \times 28$  for SVHN and  $32 \times 32$  for CelebA and CIFAR, while video experiments were performed on  $64 \times 64$  frames according to the existing protocol [13]. Further experimental details are in App. B.

Table 1: Analysis of learned variance on SVHN. The parameter  $\beta$  is tuned manually in  $\beta$ -VAE and learned in  $\sigma$ -VAE.  $\sigma$ -VAE achieves better performance, while the value of  $\beta$  (implicitly defined via the decoder variance) automatically converges close the value found by manual tuning.

|                      | $\beta$ | $-\log p \downarrow$ | FID $\downarrow$ |
|----------------------|---------|----------------------|------------------|
| $\beta$ -VAE         | 0.001   | $< 21.43$            | 44.54            |
| $\beta$ -VAE         | 0.01    | $< -3186$            | 27.93            |
| $\beta$ -VAE         | 0.1     | $< -1223$            | 28.3             |
| $\beta$ -VAE         | 1       | $< 1381$             | 70.39            |
| $\beta$ -VAE         | 10      | $< 4056$             | 219.3            |
| $\sigma$ -VAE (Ours) | 0.006   | $< -3333$            | <b>22.25</b>     |

### 5.1 Do calibrated decoders balance the VAE objective, removing the need for $\beta$ ?

As detailed in Section 3.1, a  $\beta$ -VAE with a unit variance Gaussian decoder commonly used in prior work is equivalent to a  $\sigma$ -VAE with constant, manually tuned variance. There is a simple relationship between beta and the variance:  $\sigma = \sqrt{\beta/2}$ . To compare the variance that the  $\sigma$ -VAE learns to the manually tuned variance in the case of the  $\beta$ -VAE, we compare the ELBO values and the corresponding values of  $\beta$  in Table 1. We find that learning the variance produces similar values of  $\beta$  to the manually tuned values in the  $\beta$ -VAE case, indicating that the  $\sigma$ -VAE is able to learn the balance between the two objective terms in a single training run, without hyperparameter tuning. Moreover, the  $\sigma$ -VAE outperforms the best  $\beta$ -VAE run. This



Figure 3: Analysis of learned variance on SVHN. The parameter  $\beta$  is tuned manually in  $\beta$ -VAE and learned in  $\sigma$ -VAE. Higher values of  $\beta$  cause the images to lose detail, while lower values of  $\beta$  might make samples unrealistic. The proposed optimal  $\sigma$ -VAE is able to learn the balance end-to-end, here converging to an equivalent of  $\beta$ -VAE with  $\beta = 0.006$ . This is because end-to-end learning produces better estimates of

the variance than is possible with manual search, improving the likelihood (as measured by the lower bound) and the visual quality. Figure 3 shows the qualitative results from this experiment.

We further validate our results on both single-image and sequential VAE models on a range of datasets in Table 2 and Figure 2. Single-sample ELBO values are reported, and ELBO values on discretized data are reported for discrete distributions. We observe that learning a shared variance in a Gaussian decoders (shared  $\sigma$ -VAE, Section 3.1) outperforms the naïve unit variance decoder (Gaussian VAE) as well as tuning the  $\beta$  constant for the Gaussian VAE manually. We also observe that calibrated discrete decoders, such as full categorical distribution or mixture of discretized logistics, perform better than the naïve Gaussian VAE. Using Bernoulli distribution by treating the color intensities as probabilities [17, 52] performs poorly. Our results further improve upon the sequence VAE method of Denton and Fergus [13], which uses a unit variance Gaussian with the  $\beta$ -VAE objective.

## 5.2 How does learning calibrated decoders impact the latent variable information content?

We saw above that calibrated decoders result in higher log-likelihood bounds. Are calibrated decoders also beneficial for representation learning? To study this, we evaluate the mutual information  $I_e(x; z)$  between the data  $p_d(x)$  and encoder samples  $q(z|x)$ , as well as the mismatch between the prior  $p(z)$  and the marginal encoder distribution  $m(z) = E_{p_d(x)} q(z|x)$ , measured by the marginal KL  $D_{KL}(m(z)||p(z))$ . These terms are related to the rate term of the VAE objective as follows [3]:

$$\begin{aligned} E_{p_d(x)} [D_{KL}(q(z|x)||p(z))] &= E_{p_d(x)} [D_{KL}(q(z|x)||m(z))] + D_{KL}(m(z)||p(z)) \\ &= I_e(x; z) + D_{KL}(m(z)||p(z)). \end{aligned} \quad (6)$$

That is, the rate term decomposes into the true mutual information and the marginal KL term. We want to learn expressive latent variables with high mutual information. However, doing so by tuning the  $\beta$  value relaxes the constraint that the encoder and the prior distributions match, and leads to degraded quality of samples from the prior, which creates a trade-off between expressive representations and ability to generate good samples. To compare the  $\beta$ -VAE and  $\sigma$ -VAE in terms of these quantities, we estimate the marginal KL term via Monte Carlo sampling, as proposed by Rosca et al. [49], and plot the results in Figure 4. As expected, we see that lower  $\beta$  values lead to higher mutual information. However, after a certain point, lower values of  $\beta$  also cause a significant mismatch between the marginal and the prior distributions. By calculating the “effective”  $\beta$  for the  $\sigma$ -VAE, as per Section 4, we can see that the  $\sigma$ -VAE captures an inflection point in the  $D_{KL}(m(z)||p(z))$  term, learning a representation with the highest possible MI, but without degrading sample quality. This explains the high visual quality of the optimal  $\sigma$ -VAE samples: since the marginal and the prior distributions match, the samples from the prior look similar to reconstructions, while for a  $\beta$ -VAE with low  $\beta$ , the samples from the prior are poor. We see that, in contrast to the  $\beta$ -VAE, where the mutual information is controlled by a hyperparameter, the  $\sigma$ -VAE can adjust the appropriate amount of information automatically and is able to find the setting that produces both informative latents and high quality samples.

An alternative discussion of tuning  $\beta$  is presented by Alemi et al. [3], who show that  $\beta$  controls the rate-distortion trade-off. Here, we show that the crucial trade-off also controlled by  $\beta$  is the trade-off between two components of the rate itself, which control expressivity of representations and the match between the variational and the prior distributions, respectively.

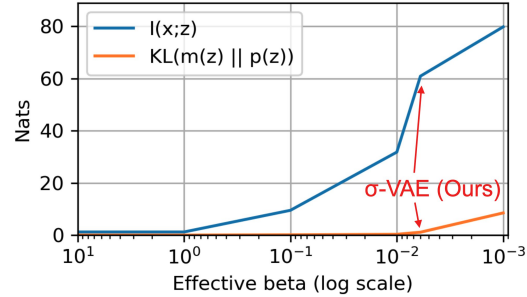


Figure 4: Comparison of  $\beta$ -VAE and  $\sigma$ -VAE on SVHN in terms of mutual information  $I_e(x; z)$  and marginal KL divergence  $KL(m(z)||p(z))$  (see Sec. 5.2).  $I_e(x; z)$  increases with lower  $\beta$ , yielding expressive representations and better reconstruction. However, after a certain point, lowering  $\beta$  leads to a rapid increase in the marginal KL, yielding poor samples from the prior. The  $\sigma$ -VAE is able to automatically find the inflection point after which the marginal KL begins to increase, capturing as much information as possible while still producing good samples.

Table 2: Generative modeling performance of the proposed  $\sigma$ -VAE on different models and datasets. For SVG, we compare with the original method [13], which uses  $\beta$ -VAE. We see that uncalibrated decoders such as mean-only Gaussian perform poorly.  $\beta$ -VAE allows to calibrate the decoder but needs careful hyperparameter tuning. Calibrated decoders such as categorical or  $\sigma$ -VAE perform best.

|                                     | CelebA HVAE          |                  | SVHN VAE             |                  | CIFAR HVAE           |                  | BAIR SVG [13]        |                  |
|-------------------------------------|----------------------|------------------|----------------------|------------------|----------------------|------------------|----------------------|------------------|
|                                     | $-\log p \downarrow$ | FID $\downarrow$ | $-\log p \downarrow$ | FID $\downarrow$ | $-\log p \downarrow$ | FID $\downarrow$ | $-\log p \downarrow$ | FID $\downarrow$ |
| Bernoulli VAE [17]                  |                      | 177.6            |                      | 43.26            |                      | 284.5            |                      | 122.6            |
| Categorical VAE                     | <b>&lt; 6359</b>     | 71.5             | < 9179               | 46.13            | <b>&lt; 7179</b>     | <b>101.7</b>     | N/A                  | N/A              |
| bitwise-categorical VAE             | < 9067               | 66.61            | < 10800              | 33.84            | < 9390               | <b>91.2</b>      | < 48744              | 46.13            |
| Logistic mixture VAE                | < 7932               | 65.3             | <b>&lt; 9085</b>     | 43.19            | < 8443               | 143.1            | <b>&lt; 40616</b>    | 42.94            |
| Gaussian VAE                        | < 7173               | 186.5            | < 2184               | 112.5            | < 7186               | 293.7            | < -10379             | 35.64            |
| Student-t VAE                       | < -8401              | 71.06            | -                    | -                | < -7419              | 123.6            | -                    | -                |
| $\beta$ -VAE [26]                   | < -2713              | <b>61.6</b>      | < -3186              | 27.93            | < -331               | <b>103</b>       | < -13472             | 34.64            |
| Shared $\sigma$ -VAE (Ours)         | < -6374              | <b>60.7</b>      | <b>&lt; -3349</b>    | <b>22.25</b>     | < -5435              | 116.1            | < -13974             | 34.24            |
| Optimal $\sigma$ -VAE (Ours)        | <b>&lt; -8446</b>    | <b>60.3</b>      | <b>&lt; -3333</b>    | 27.25            | <b>&lt; -5677</b>    | <b>101.4</b>     | <b>&lt; -14173</b>   | 34.13            |
| Opt. per-image $\sigma$ -VAE (Ours) |                      | 66.01            |                      | 26.28            |                      | <b>104.0</b>     |                      | <b>33.21</b>     |

### 5.3 What are the common challenges in learning the variance that prevent practitioners from using it, and how to rectify them?

If learning the decoder variance improves generation, why are learned variances not used more often? In this section, we discuss how the naïve approach to learning variances, where the decoder outputs a variance for each pixel along with the mean, leads to poor results. First, we find that this method often diverges very quickly due to numerical instability, as the network is able to predict certain pixels with very high certainty, leading to degenerate variances. In contrast, learning a shared variance is always numerically stable in our experiments. We can rectify this numerical instability by bounding the output variance (Section 3.1). However, even with bounded variance, we observe that learning per-pixel variances leads to poor results in Table 3. While the per-pixel variance achieves a good ELBO value, it produces very poor samples, as measured by FID and visual inspection. We hypothesize that the per-pixel decoder allocates significant capacity to learning the variance, which prevents it from learning to produce good samples.

Table 3: Ablation on the MNIST dataset. The naïve calibrated decoder with per-pixel variance surprisingly performs poorly. However, calibrated decoders such as Bernoulli or shared  $\sigma$ -VAE perform best, improving over uncalibrated decoders.

|                             | $-\log p \downarrow$ | FID $\downarrow$ |
|-----------------------------|----------------------|------------------|
| Gaussian VAE                | < 740.5              | 59.9             |
| $\beta$ -VAE                | < -796.2             | 53.23            |
| Per-pixel $\sigma$ -VAE     | < -2895              | 132.5            |
| Shared $\sigma$ -VAE (Ours) | < -896.1             | <b>32.18</b>     |
| Bernoulli VAE               |                      | <b>32.22</b>     |

### 5.4 Can an analytic solution for optimal variance further improve learning?

We evaluate the *optimal*  $\sigma$ -VAE which uses an analytic solution for the variance (Section 4). Table 2 shows that it achieves superior results in terms of log-likelihood. We also note that the optimal  $\sigma$ -VAE converges to a good variance estimate instantaneously, which speeds up learning (highlighted in Figure 9 in the Appendix). In addition, we evaluate the per-image optimal  $\sigma$ -VAE, in which a single variance is computed per image. This model achieves significantly higher visual quality. While producing this per-image variance with a neural network would require additional architecture tuning, optimal  $\sigma$ -VAE is extremely simple to implement (it can be implemented simply as changing the axes of summation), not requiring any new tunable parameters.

## 6 Conclusion

We presented a simple and effective method for learning calibrated decoders, as well as an evaluation of different decoding distributions with several VAE and sequential VAE models. The proposed method outperforms methods that use naïve unit variance Gaussian decoders and tune a heuristic weight  $\beta$  on the KL-divergence loss, as commonly done in prior work. Moreover, it does not use the heuristic weight  $\beta$ , making it easier to train than this prior work. We expect that the simple techniques for learning calibrated decoders can allow practitioners to speed up the development cycle, obtain better results, and reduce the need for manual hyperparameter tuning.



## 7 Acknowledgements

We thank Vagelis Chatzipantazis, Marvin Zhang, Vitchyr Pong, Rahul Ramesh and Danijar Hafner for fruitful discussions, and Karl Pertsch for feedback on the Sequential VAE setting. We also thank Rahul Ramesh, Coline Devin, Michael Janner, and Justin Fu on feedback on an earlier version of the paper. This work was supported through the following grants: NSF-IIP-1439681 (I/UCRC), NSF-IIS-1703319, NSF MRI 1626008, ARL RCTA W911NF-10-2-0016, ONR N00014-17-1-2093, ARL DCIST CRA W911NF-17-2-0181, the DARPA-SRC C-BRIC, and by Honda Research Institute.

## References

- [1] Martín Abadi, Paul Barham, Jianmin Chen, Zhifeng Chen, Andy Davis, Jeffrey Dean, Matthieu Devin, Sanjay Ghemawat, Geoffrey Irving, Michael Isard, et al. Tensorflow: A system for large-scale machine learning. In 12th {USENIX} Symposium on Operating Systems Design and Implementation ({OSDI} 16), pages 265–283, 2016.
- [2] Alessandro Achille and Stefano Soatto. Information dropout: Learning optimal representations through noisy computation. IEEE transactions on pattern analysis and machine intelligence, 40(12):2897–2905, 2018.
- [3] Alexander A Alemi, Ben Poole, Ian Fischer, Joshua V Dillon, Rif A Saurous, and Kevin Murphy. Fixing a broken elbo. arXiv preprint arXiv:1711.00464, 2017.
- [4] Shun-Ichi Amari. Natural gradient works efficiently in learning. Neural computation, 10(2): 251–276, 1998.
- [5] Georgios Arvanitidis, Lars Kai Hansen, and Søren Hauberg. Latent space oddity: on the curvature of deep generative models. arXiv preprint arXiv:1710.11379, 2017.
- [6] Mohammad Babaeizadeh, Chelsea Finn, Dumitru Erhan, Roy H. Campbell, and Sergey Levine. Stochastic variational video prediction. 2018.
- [7] Samuel R Bowman, Luke Vilnis, Oriol Vinyals, Andrew Dai, Rafal Jozefowicz, and Samy Bengio. Generating sentences from a continuous space. In Proceedings of The 20th SIGNLL Conference on Computational Natural Language Learning, pages 10–21, 2016.
- [8] Lluís Castrejón, Nicolas Ballas, and Aaron Courville. Improved conditional vrnnns for video prediction. In Proceedings of the IEEE International Conference on Computer Vision, pages 7608–7617, 2019.
- [9] Xi Chen, Diederik P Kingma, Tim Salimans, Yan Duan, Prafulla Dhariwal, John Schulman, Ilya Sutskever, and Pieter Abbeel. Variational lossy autoencoder. arXiv preprint arXiv:1611.02731, 2016.
- [10] Kurtland Chua, Roberto Calandra, Rowan McAllister, and Sergey Levine. Deep reinforcement learning in a handful of trials using probabilistic dynamics models. In Advances in Neural Information Processing Systems, pages 4754–4765, 2018.
- [11] Junyoung Chung, Kyle Kastner, Laurent Dinh, Kratarth Goel, Aaron C Courville, and Yoshua Bengio. A recurrent latent variable model for sequential data. 2015.
- [12] Bin Dai and David Wipf. Diagnosing and enhancing vae models. arXiv preprint arXiv:1903.05789, 2019.
- [13] E. Denton and R. Fergus. Stochastic video generation with a learned prior. 2018.
- [14] Prafulla Dhariwal, Heewoo Jun, Christine Payne, Jong Wook Kim, Alec Radford, and Ilya Sutskever. Jukebox: A generative model for music. arXiv preprint arXiv:[TODO], 2020.
- [15] Harrison Edwards and Amos Storkey. Towards a neural statistician. arXiv preprint arXiv:1606.02185, 2016.
- [16] Chelsea Finn and Sergey Levine. Deep visual foresight for planning robot motion. 2017.
- [17] Karol Gregor, Ivo Danihelka, Alex Graves, Danilo Jimenez Rezende, and Daan Wierstra. Draw: A recurrent neural network for image generation. arXiv preprint arXiv:1502.04623, 2015.
- [18] Karol Gregor, Frederic Besse, Danilo Jimenez Rezende, Ivo Danihelka, and Daan Wierstra. Towards conceptual compression. 2016.

- [19] Karol Gregor, George Papamakarios, Frederic Besse, Lars Buesing, and Theophane Weber. Temporal difference variational auto-encoder. 2019.
- [20] Ishaan Gulrajani, Kundan Kumar, Faruk Ahmed, Adrien Ali Taiga, Francesco Visin, David Vazquez, and Aaron Courville. Pixelvae: A latent variable model for natural images. arXiv preprint arXiv:1611.05013, 2016.
- [21] David Ha and Douglas Eck. A neural representation of sketch drawings. arXiv preprint arXiv:1704.03477, 2017.
- [22] Danijar Hafner, Timothy Lillicrap, Jimmy Ba, and Mohammad Norouzi. Dream to control: Learning behaviors by latent imagination. arXiv preprint arXiv:1912.01603, 2019.
- [23] Danijar Hafner, Timothy Lillicrap, Ian Fischer, Ruben Villegas, David Ha, Honglak Lee, and James Davidson. Learning latent dynamics for planning from pixels. 2019.
- [24] Mikael Henaff, Alfredo Canziani, and Yann LeCun. Model-predictive policy learning with uncertainty regularization for driving in dense traffic. arXiv preprint arXiv:1901.02705, 2019.
- [25] Martin Heusel, Hubert Ramsauer, Thomas Unterthiner, Bernhard Nessler, and Sepp Hochreiter. Gans trained by a two time-scale update rule converge to a local nash equilibrium. In Advances in neural information processing systems, pages 6626–6637, 2017.
- [26] Irina Higgins, Loic Matthey, Arka Pal, Christopher Burgess, Xavier Glorot, Matthew Botvinick, Shakir Mohamed, and Alexander Lerchner. beta-VAE: Learning basic visual concepts with a constrained variational framework. 2017.
- [27] Michael I Jordan, Zoubin Ghahramani, Tommi S Jaakkola, and Lawrence K Saul. An introduction to variational methods for graphical models. Machine learning, 37(2):183–233, 1999.
- [28] Diederik P Kingma and Jimmy Ba. Adam: A method for stochastic optimization. 2015.
- [29] Diederik P Kingma and Max Welling. Auto-encoding variational Bayes. 2014.
- [30] Durk P Kingma, Tim Salimans, Rafal Jozefowicz, Xi Chen, Ilya Sutskever, and Max Welling. Improved variational inference with inverse autoregressive flow. In Advances in neural information processing systems, pages 4743–4751, 2016.
- [31] Simon Kohl, Bernardino Romera-Paredes, Clemens Meyer, Jeffrey De Fauw, Joseph R Led- sam, Klaus Maier-Hein, SM Ali Eslami, Danilo Jimenez Rezende, and Olaf Ronneberger. A probabilistic u-net for segmentation of ambiguous images. In Advances in Neural Information Processing Systems, pages 6965–6975, 2018.
- [32] Alex Krizhevsky, Geoffrey Hinton, et al. Learning multiple layers of features from tiny images. 2009.
- [33] A. X. Lee, R. Zhang, F. Ebert, P. Abbeel, C. Finn, and S. Levine. Stochastic adversarial video prediction. arXiv:1804.01523, abs/1804.01523, 2018.
- [34] Alex X Lee, Anusha Nagabandi, Pieter Abbeel, and Sergey Levine. Stochastic latent actor-critic: Deep reinforcement learning with a latent variable model. arXiv preprint arXiv:1907.00953, 2019.
- [35] Ziwei Liu, Ping Luo, Xiaogang Wang, and Xiaoou Tang. Deep learning face attributes in the wild. In Proceedings of International Conference on Computer Vision (ICCV), December 2015.
- [36] James Lucas, George Tucker, Roger B Grosse, and Mohammad Norouzi. Don’t blame the elbo! a linear vae perspective on posterior collapse. In Advances in Neural Information Processing Systems, pages 9403–9413, 2019.
- [37] Lars Maaløe, Marco Fraccaro, Valentin Liévin, and Ole Winther. Biva: A very deep hierarchy of latent variables for generative modeling. In Advances in neural information processing systems, pages 6548–6558, 2019.
- [38] Pierre-Alexandre Mattei and Jes Frellsen. Leveraging the exact likelihood of deep latent variable models. In Advances in Neural Information Processing Systems, pages 3855–3866, 2018.
- [39] Radford M Neal and Geoffrey E Hinton. A view of the em algorithm that justifies incremental, sparse, and other variants. In Learning in graphical models, pages 355–368. Springer, 1998.

- [40] Yuval Netzer, Tao Wang, Adam Coates, Alessandro Bissacco, Bo Wu, and Andrew Y Ng. Reading digits in natural images with unsupervised feature learning. 2011.
- [41] Adam Paszke, Sam Gross, Francisco Massa, Adam Lerer, James Bradbury, Gregory Chanan, Trevor Killeen, Zeming Lin, Natalia Gimelshein, Luca Antiga, et al. Pytorch: An imperative style, high-performance deep learning library. In Advances in Neural Information Processing Systems, pages 8024–8035, 2019.
- [42] Georgios Pavlakos, Vasileios Choutas, Nima Ghorbani, Timo Bolkart, Ahmed AA Osman, Dimitrios Tzionas, and Michael J Black. Expressive body capture: 3d hands, face, and body from a single image. In Proceedings of the IEEE Conference on Computer Vision and Pattern Recognition, pages 10975–10985, 2019.
- [43] Xue Bin Peng, Angjoo Kanazawa, Sam Toyer, Pieter Abbeel, and Sergey Levine. Variational discriminator bottleneck: Improving imitation learning, inverse rl, and gans by constraining information flow. arXiv preprint arXiv:1810.00821, 2018.
- [44] Jan Peters and Stefan Schaal. Reinforcement learning of motor skills with policy gradients. Neural networks, 21(4):682–697, 2008.
- [45] Vitchyr H Pong, Murtaza Dalal, Steven Lin, Ashvin Nair, Shikhar Bahl, and Sergey Levine. Skew-fit: State-covering self-supervised reinforcement learning. arXiv preprint arXiv:1903.03698, 2019.
- [46] Danilo Jimenez Rezende and Fabio Viola. Taming vaes. arXiv preprint arXiv:1810.00597, 2018.
- [47] Danilo Jimenez Rezende, Shakir Mohamed, and Daan Wierstra. Stochastic backpropagation and approximate inference in deep generative models. 2014.
- [48] Jason Tyler Rolfe. Discrete variational autoencoders. arXiv preprint arXiv:1609.02200, 2016.
- [49] Mihaela Rosca, Balaji Lakshminarayanan, and Shakir Mohamed. Distribution matching in variational inference. arXiv preprint arXiv:1802.06847, 2018.
- [50] Tim Salimans, Andrej Karpathy, Xi Chen, and Diederik P Kingma. Pixelcnn++: Improving the pixelcnn with discretized logistic mixture likelihood and other modifications. arXiv preprint arXiv:1701.05517, 2017.
- [51] Casper Kaae Sønderby, Tapani Raiko, Lars Maaløe, Søren Kaae Sønderby, and Ole Winther. Ladder variational autoencoders. In Advances in neural information processing systems, pages 3738–3746, 2016.
- [52] Manuel Watter, Jost Springenberg, Joshka Boedecker, and Martin Riedmiller. Embed to control: A locally linear latent dynamics model for control from raw images. In Advances in neural information processing systems, pages 2746–2754, 2015.
- [53] Shengjia Zhao, Jiaming Song, and Stefano Ermon. Infovae: Information maximizing variational autoencoders. arXiv preprint arXiv:1706.02262, 2017.
- [54] Jun-Yan Zhu, Richard Zhang, Deepak Pathak, Trevor Darrell, Alexei A Efros, Oliver Wang, and Eli Shechtman. Toward multimodal image-to-image translation. In Advances in neural information processing systems, pages 465–476, 2017.



Figure 5: Samples from the  $\sigma$ -VAE (left) and the Gaussian VAE (right) on the SVHN dataset. The Gaussian VAE produces blurry results with muted colors, while the  $\sigma$ -VAE is able to produce accurate images of digits.



Figure 6: Samples from the  $\sigma$ -VAE (left) and the Gaussian VAE (right) on the CelebA dataset, images cropped to the face for clarity. The Gaussian VAE produces blurry results with indistinct face features, while the  $\sigma$ -VAE is able to produce accurate images of faces.

## A Additional experimental results

In this section, we provide more qualitative results in Figures 7, 6, 8, 5 as well as a graph showing the convergence properties of the variance for different models in Fig. 9. In order to validate our method with a different architecture, we also report performance of different decoders with a small 5-layer convolutional architecture on the CelebA and CIFAR dataset in Table 4. We see that the ordering of the methods is consistent with this smaller architecture.

## B Experimental details

For the small convolutional network test on SVHN, the encoder has 3 convolutional layers followed by a fully connected layer, while the decoder has a fully connected layer followed by 3 convolutional layers. The  $\beta$  was tuned from 100 to 0.0001 for  $\beta$ -VAE. The number of channels in the convolutional layers starts with 32 and increases 2 times in every layer. The dimension of the latent variable is 20. Adam [28] with learning rate of  $1e-3$  is used for optimization. Batch size of 128 was used and all models were trained for 10 epochs. We additionally evaluate this small convolutional network on



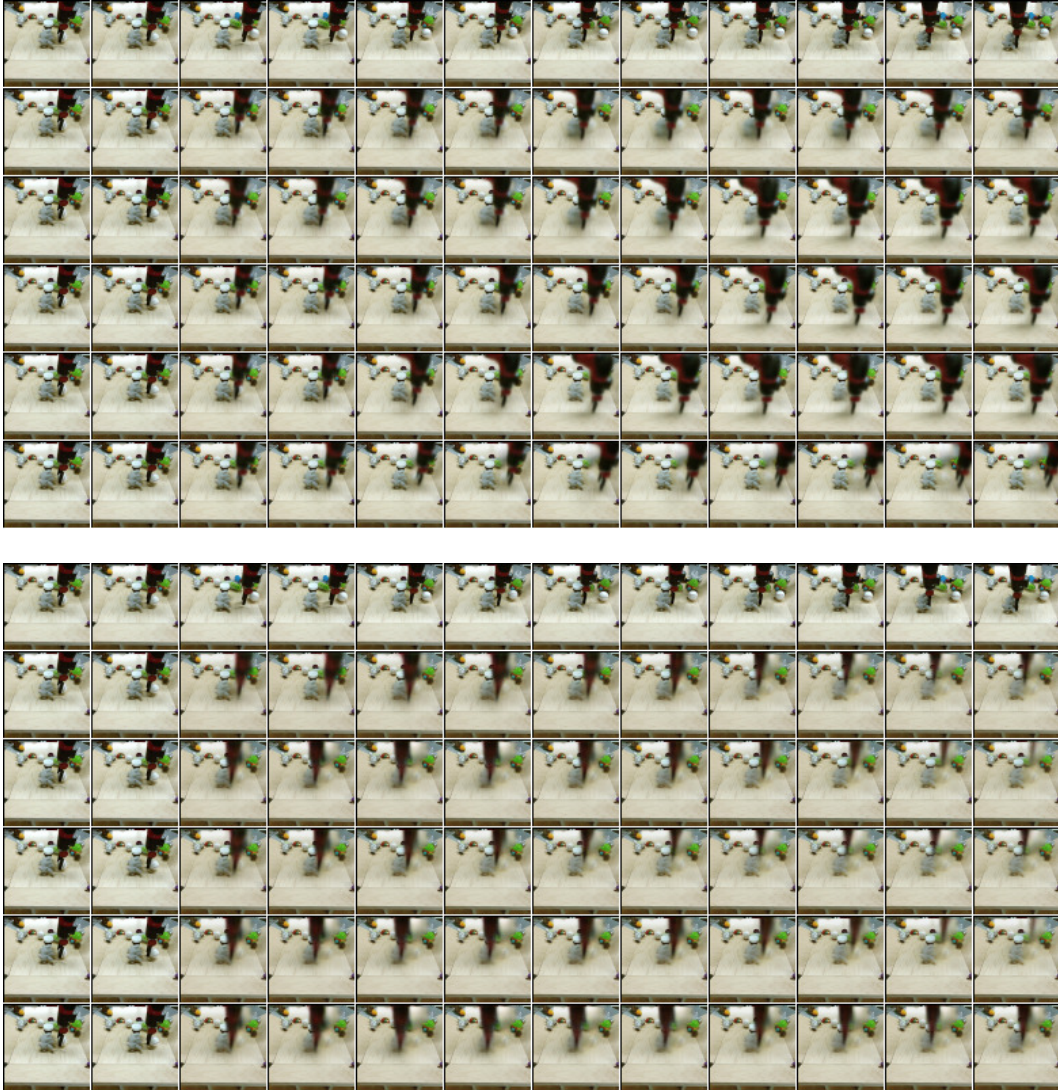


Figure 7: Samples from the  $\sigma$ -VAE (top) and the Gaussian VAE (bottom) on the BAIR dataset. Sampled sequences conditioned on two initial frames are shown, and the ground truth sequence is shown at the top. The Gaussian VAE produces blurry robot arm texture and the arm often disappears towards the end of the sequence, while the  $\sigma$ -VAE is able to produce sequences with realistic motion and model the details of the arm texture, such as the gripper.

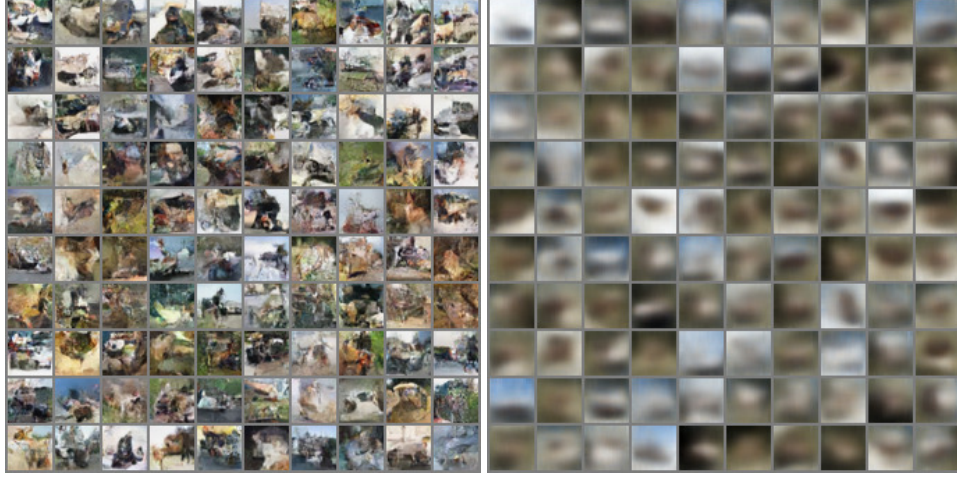


Figure 8: Samples from the  $\sigma$ -VAE (left) and the Gaussian VAE (right) on the challenging CIFAR dataset. The Gaussian VAE produces blurry results with muted colors, while the  $\sigma$ -VAE models the distribution of shapes in the CIFAR data more faithfully.

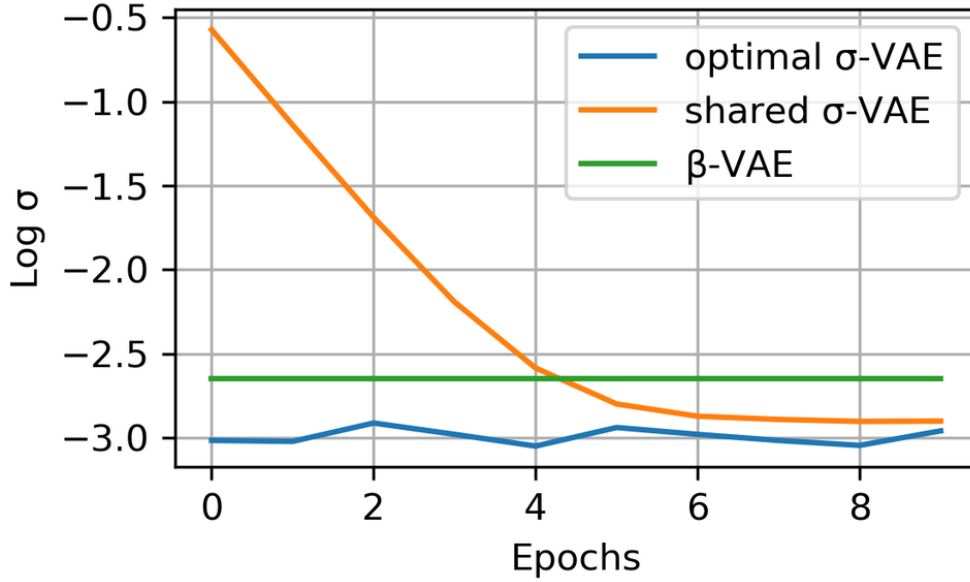


Figure 9: Variance convergence speed on SVHN. We see that the shared  $\sigma$ -VAE which optimizes the variance with gradient descent has an initial period of convergence when the variance converges to the region of the optimal value. In contrast,  $\sigma$ -VAE with analytical (optimal) variance quickly learns a good estimate of the variance, which leads to better performance. The unit variance Gaussian  $\beta$ -VAE can be interpreted as having a constant variance determined by  $\beta$ , shown here. Since the variance doesn't change throughout training, it achieves suboptimal performance.

Table 4: Generative modeling performance of the proposed  $\sigma$ -VAE on CelebA, CIFAR, and Frey Face with a smaller model. We see that uncalibrated decoders such as mean-only Gaussian perform poorly.  $\beta$ -VAE allows to calibrate the decoder but needs careful hyperparameter tuning. Calibrated decoders such as categorical or  $\sigma$ -VAE perform best.

|                                     | CelebA VAE           |                  | CIFAR VAE            |                  | Frey Face VAE        |                  |
|-------------------------------------|----------------------|------------------|----------------------|------------------|----------------------|------------------|
|                                     | $-\log p \downarrow$ | FID $\downarrow$ | $-\log p \downarrow$ | FID $\downarrow$ | $-\log p \downarrow$ | FID $\downarrow$ |
| Bernoulli VAE [17]                  |                      | 102.7            |                      | 165.1            |                      | 47.7             |
| Categorical VAE                     | <10195               | <b>50.45</b>     | <10673               | 124.1            | < <b>2454</b>        | 50.16            |
| bitwise-categorical VAE             | 11019                | 56.36            | 11604                | 99.65            | < 3173               | 66.77            |
| Logistic mixture VAE                | < <b>10154</b>       | 61.81            | < <b>10648</b>       | 100.2            | < 2562               | 50.28            |
| Gaussian VAE                        | < 2201               | 144.8            | < 1409               | 205.8            | < 726.4              | 80.17            |
| $\beta$ -VAE [26]                   | < <b>-1942</b>       | 58.73            | < -1318              | 117.9            | < -420.0             | <b>37.61</b>     |
| Shared $\sigma$ -VAE (Ours)         | < <b>-1939</b>       | 73.27            | < <b>-1830</b>       | 137.8            | < -49.78             | <b>42.86</b>     |
| Optimal $\sigma$ -VAE (Ours)        | < <b>-1951</b>       | 61.27            | < <b>-1832</b>       | <b>80.9</b>      | < <b>-1622</b>       | 53.36            |
| Opt. per-image $\sigma$ -VAE (Ours) |                      | <b>53.13</b>     |                      | 89.88            |                      | 56.07            |

CelebA, CIFAR, and Frey Face<sup>3</sup> datasets in Table 4. Unit Gaussian prior and Gaussian posteriors with diagonal covariance were used. For the larger hierarchical VAE, we used the official pytorch implementation of [37]. We use the baseline hierarchical VAE with 15 layers of latent variables, without the top-down and bottom-up connections. For the hierarchical VAE and the SVG-LP model, we use the default hyperparameters in the respective implementations. We use the standard train-val-test split for all datasets. All models were trained on a single high-end GPU. We use the official PyTorch implementation of the Inception network to compute FID. All methods are compared on the same hyperparameters.

## C Alternative Decoder Choices

We describe the alternative decoders evaluated in Table 2: using the bitwise-categorical, and the logistic mixture distributions.

**Bitwise-categorical VAE** While the 256-way categorical decoder described in Section 3.2 is very powerful due to the ability to specify any possible intensity distribution, it suffers from high computational and memory requirements. Because 256 values need to be kept for each pixel and channel, simply keeping this distribution in memory for one 3-channel  $1024 \times 1024$  image would require 3 GiB of memory, compared to 0.012 GiB for the Gaussian decoder. Therefore, training deep neural networks with this full categorical distribution is impractical for high-resolution images or videos. The bitwise-categorical VAE improves the memory complexity by defining the distribution over 256 values in a more compact way. Specifically, it defines a binary distribution over each bit in the pixel intensity value, requiring 8 values in total, one for each bit. This distribution can be thought of as a classifier that predicts the value of each bit in the image separately. In our implementation of the bitwise-categorical likelihood, we convert the image channels to binary format and use the standard binary cross-entropy loss (which reduces to binary log-likelihood since all bits in the image

Table 5: ELBO on discretized data. All distributions except categorical have scalar scale parameters. The  $\sigma$ -VAE performs well on the discretized ELBO metric, performing similarly to a discrete distribution parametrized as a discretized Gaussian or discretized Logistic. Full categorical distribution attains highest likelihood due to having the most statistical power.

|                              | CIFAR VAE                     |                      |                  |
|------------------------------|-------------------------------|----------------------|------------------|
|                              | $-\log \text{pdf} \downarrow$ | $-\log p \downarrow$ | FID $\downarrow$ |
| Categorical VAE              |                               | < <b>10673</b>       | <b>137.6</b>     |
| Gaussian VAE                 | < 740.5                       | < 15131              | 212.7            |
| Gaussian $\sigma$ -VAE       | < -896.1                      | < 11120              | <b>136.7</b>     |
| Disc. Gaussian $\sigma$ -VAE |                               | < 11117              | <b>136.9</b>     |
| Disc. Logistic $\sigma$ -VAE |                               | < 11103              | <b>136.7</b>     |

<sup>3</sup>Available at <https://cs.nyu.edu/~roweis/data.html>

are deterministically either zero or one). While in our experiments the bitwise-categorical distribution did not outperform other choices, it often performs on par with our proposed method. We expect this distribution to be useful due to its generality as it is able to represent values stored in any digital format by converting them into binary.

**Logistic mixture VAE** For this decoder, we adapt the discretized logistic mixture from Salimans et al. [50]. To define a discrete 256-way distribution, it divides the corresponding continuous distribution into 256 bins, where the probability mass is defined as the integral of the PDF over the corresponding bin. [30] uses the logistic distribution discretized in this manner for the decoder. Salimans et al. [50] suggests to make all bins except the first and the last be of equal size, whereas the first and the last bin include, respectively, the intervals  $(-\infty, 0]$  and  $[1, \infty)$ . Salimans et al. [50] further suggests using a mixture of discretized logistics for improved capacity. Our implementation largely follows the one in Salimans et al. [50], however, we note that the original implementation is not suitable for learning latent variable models, as it generates the channels autoregressively. This will cause the latent variable to lose color information since it can be represented by the autoregressive decoder. We therefore adapt the mixture of discretized logistics to the pure latent variable setup by removing the mean-adjusting coefficients from [50]. In our experiments, the logistic mixture outperformed other discrete distributions.